Scanning Tunneling Microscopy and Atomic Force Microscopy: Application to Biology and Technology

P. K. HANSMA, V. B. ELINGS, O. MARTI, C. E. BRACKER

The scanning tunneling microscope (STM) and the atomic force microscope (AFM) are scanning probe microscopes capable of resolving surface detail down to the atomic level. The potential of these microscopes for revealing subtle details of structure is illustrated by atomic resolution images including graphite, an organic conductor, an insulating layered compound, and individual adsorbed oxygen atoms on a semiconductor. Application of the STM for imaging biological materials directly has been hampered by the poor electron conductivity of most biological samples. The use of thin conductive metal coatings and replicas has made it possible to image some biological samples, as indicated by recently obtained images of a recA-DNA complex, a phospholipid bilayer, and an enzyme crystal. The potential of the AFM, which does not require a conductive sample, is shown with molecular resolution images of a nonconducting organic monolayer and an amino acid crystal that reveals individual methyl groups on the ends of the amino acids. Applications of these new microscopes to technology are demonstrated with images of an optical disk stamper, a diffraction grating, a thin-film magnetic recording head, and a diamond cutting tool. The STM has even been used to improve the quality of diffraction gratings and magnetic recording heads.

THE SCANNING TUNNELING MICROSCOPE (STM) (*1–4*) AND the atomic force microscope (AFM) (*5, 6*) are redefining the concept of microscopy and giving rise to an emerging family of scanning probe microscopes (*7*). These instruments have attracted special attention from physicists, engineers, and now biologists because they can resolve surface detail down to the atomic level with seemingly nondestructive probes (*8–10*). The main inspiration for this generation of new microscopes came from the work of Binnig and Rohrer, who received the 1986 Nobel Prize in Physics (*11*) for inventing the STM. The award was presented only 4 years after the first publication of the STM technique, signaling the perceived importance of this new instrument. The STM can image surfaces of substances that readily conduct electrons, and as a result much has been revealed about the atomic organization of materials such as silicon (*12*), gallium arsenide (*13*), and graphite (*14*), among others. More recently, Binnig, Quate, and Gerber (*5*) invented the AFM, a first-generation descendent of the STM that can image nonconducting as well as conducting surfaces.

Scanning tunneling microscopes are already being used in more than 100 laboratories and can even be purchased from several commercial sources (*15, 16*). Atomic force microscopes, however, are still in the early stages of development; they have been operated in fewer than ten laboratories worldwide and have not yet been developed to a level that permits routine use.

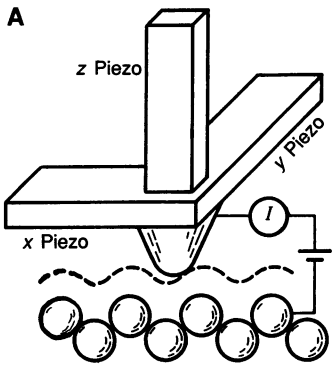

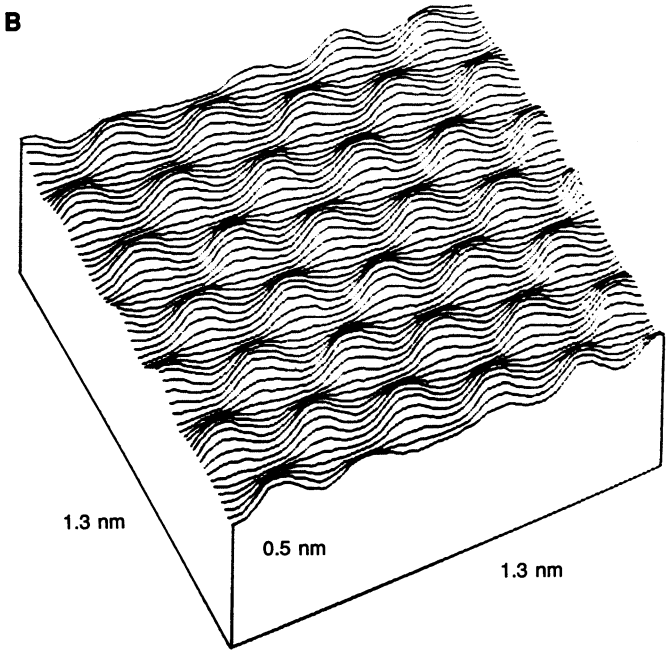

Fig. 1. (**A**) Schematic view of an STM. The tip, shown as a rounded cone, is mounted on a piezoelectric *x*, *y*, *z* scanner. A scan (dashed line) of the tip over the sample can reveal contours of the surface down to the atomic level. (**B**) An STM image showing carbon atoms in a sample of highly oriented pryolytic graphite. This is a line scan image displayed as a viewer 45° above the surface would see it. An STM image is made up of a series of line scans, each displaced in *y* from the previous one, and displays the path the tip followed over the surface.

P. K. Hansma, V. B. Elings, and O. Marti are at the Department of Physics, University of California, Santa Barbara, CA 93106. C. E. Bracker is at the Department of Botany and Plant Pathology, Purdue University, West Lafayette, IN 47907.

The Scanning Tunneling Microscope

The principles and operation of an STM are surprisingly simple. As shown schematically (Fig. 1A), an extremely sharp conductive tip (ideally terminating in a single atom) traces the contours of a surface with atomic resolution. The tip can be moved in three dimensions with an x, y, z piezoelectric translator (*17*). If the piezoelectric element is calibrated to move 1 nm for every volt applied to it, then the tip will scan over approximately three atoms as the potential applied to the piezo changes by 1 V.

The distance between the tip and the surface of the sample is controlled by a voltage applied to the z piezo element. The voltage is determined by a feedback circuit that measures and controls a small electrical current I caused by electrons tunneling across the gap between the tip and the sample under the influence of a low bias voltage applied to the tip (typically a few millivolts to a few volts). As the x piezo scans the tip laterally across the surface, the feedback circuit adjusts the voltage to the z piezo, which raises and lowers the tip to keep the tunneling current constant. The size of the tunneling current is very sensitive to the distance (height) between the tip and the sample surface; that distance does not exceed a few nanometers. Typically, the tunneling current will change by a factor of 2 or greater for a change in the distance between the tip and the surface of 0.1 nm.

Because the tunneling current is so sensitive to the separation of the tip and sample, differences in height along the contours (dashed line in Fig. 1A) can be revealed to better than 1/100 of an atomic diameter. The lateral resolution along the contours, however, is determined by the radius of curvature of the tip. A tip terminating in a single atom will have atomic resolution.

A single scan records the voltage applied to the z piezo as a function of the voltage applied to the x piezo. A complete image is made up of multiple scans, each displaced from the preceding scan by a small shift in the y direction to create a raster pattern (Fig. 1B). Note that in this real STM image, the tip goes over an atom in one scan, between atoms a few scans later, and then over the next atom. With computer-based image processing the data from such scans can be transformed into striking images that reveal topography as gray-level detail, illuminated filled surfaces, or pseudo-colored elevation maps. A full range of noise filtering, averaging, and transform routines can enhance images by minimizing noise, eliminating systematic errors, and emphasizing periodic structure.

In practice, the size of the raster pattern, the scanning rate, and many other operational variables can be varied. Piezo translators of various ranges have been designed so that scanning ranges from less than a nanometer to more than 10 μm are possible. With scanning

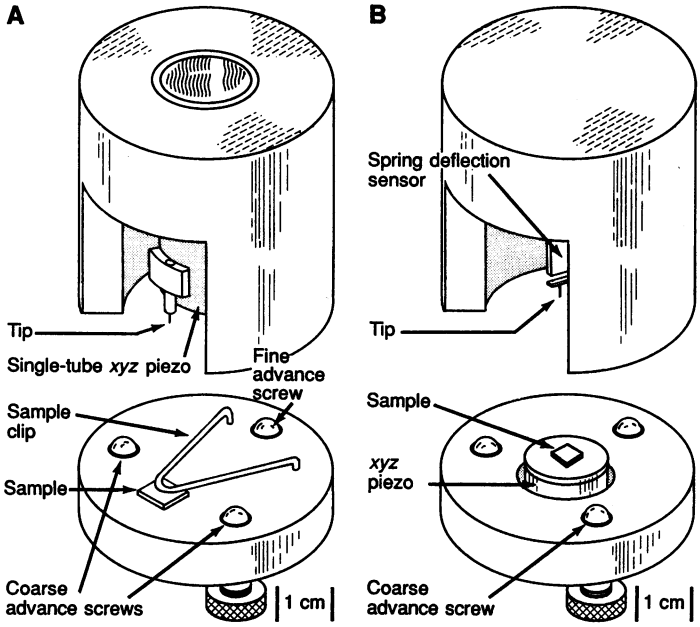

Fig. 2. (**A**) Drawing of an actual STM head and base showing the essential components. Also depicted are the three screws used for controlling the mechanical approach of the tip to the surface. Three keys to a successful STM design are (i) a smooth mechanical approach mechanism, (ii) rigidity, and (iii) convenience in changing sample and tip. (**B**) Drawing of a combination AFM-STM in which the sample moves rather than the tip. This allows the delicate force sensor, shown schematically in Fig. 6B, to be stationary. If the force sensor is replaced with a metal tip, the instrument becomes an STM. The mechanical approach system for advancing the tip toward the sample is similar to that shown in (A).

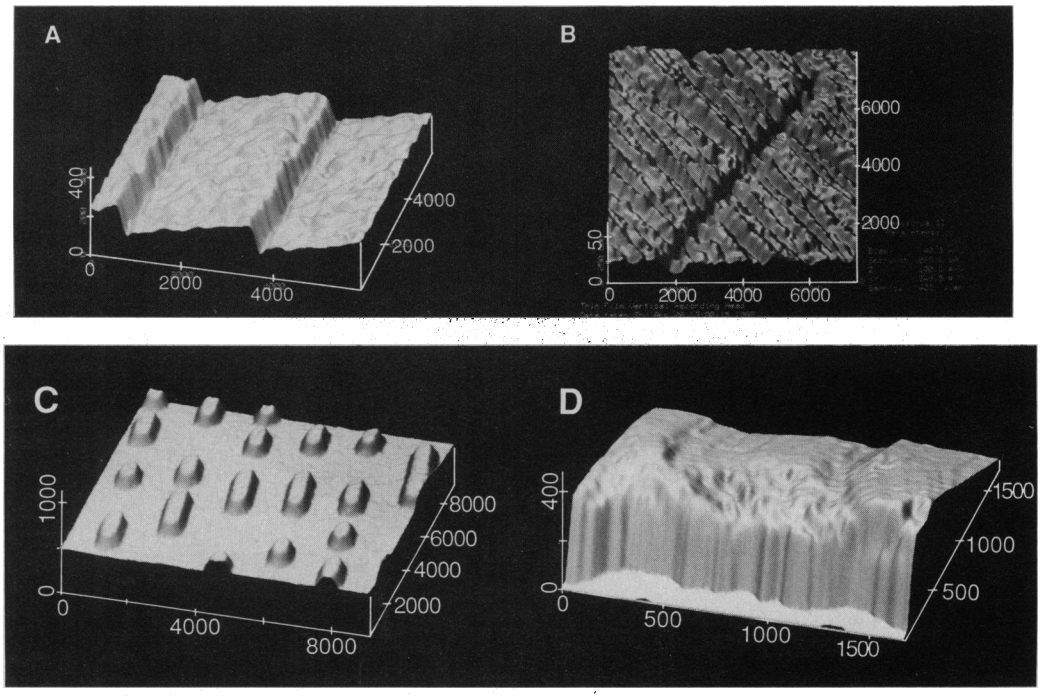

Fig. 3. Examples of technological applications of the STM. (**A**) A 6 μm by 6 μm scan of a gold diffraction-grating master (*21*). The grating is 375 lines per millimeter, and the steps are 120 nm high. (**B**) A thin-film magnetic recording head (*22*). The magnetic material is about 0.5 μm wide. Measurements show that the material is undercut about 20 nm below the surrounding material during lapping. (**C**) Bumps on a compact disk stamper (*23*). Five tracks are shown in this image. (**D**) The sharpened edge of a diamond cutting tool (*24*). The diamond is a type 2B blue diamond, which is conductive enough for the STM to image. The scales in all of these figures are in nanometers.

ranges extended into the micrometer range, structural information can now be obtained that extends from the atomic scale well into the range that is visible with light microscopes. This advance significantly extends the range and versatility of these new microscopes for technological and biological applications.

There have been many designs for STMs. As an example, Fig. 2A shows one that we have developed and used (*18*). The x, y, and z tripod of piezos in the schematic view of Fig. 1A has been replaced with a single-tube xyz piezo (*19*). The electrodes on the single tube are divided into segments that are driven with the voltages for $+x$, $-x$, $+y$, $-y$, and z. The advantage of the single-tube scanner is that it is more rigid and thus less sensitive to vibration than typical tripod designs. The microscope has three screws (*18, 20*) for advancing the tip close enough to the sample to be within range of the single-tube xyz piezo. The operator turns the two coarse advance screws by hand and watches the tip with a low-power microscope (×10 to ×30) until it is within ~10 μm of the sample. A stepping motor coupled to the fine advance screw then brings the tip the rest of the way to the sample. The motion of the fine advance screw is demagnified by a factor of order 10, since it pivots the top piece around an axis formed by the two coarse advance screws; the tip and sample are only a tenth as far from this axis as the fine advance screw.

Applications of the STM in Technology

Although much of the excitement concerning the STM is focused on its ability to image objects on the atomic and molecular scale, the STM also emerges as a singular device for mapping and measuring three-dimensional surface profiles of objects in the range from 0.01 to 10 μm. This lateral size range is well within the resolution capability of scanning electron microscopes (SEM), but an SEM has poor capability for measuring vertical distances. Here the STM excels and can even maintain 1-nm vertical resolution over scan sizes as large as 8 μm.

One of the first industrial applications of an STM is shown in the shaded surface image of a gold diffraction-grating master (Fig. 3A). This grating has 375 grooves per millimeter with a blaze angle of 3°. The sawtooth steps are 120 nm high. The instrument that can best measure these vertical profiles over micrometer scan ranges is the STM. A commercial STM was used to guide the manufacture of this grating master (*21*) and to adjust the ruling machine to produce a nearly flat blaze.

Another recent application of the STM is in understanding and improving the manufacture of vertical recording thin-film magnetic recording heads (*22*). During manufacture, the layered head is lapped smooth, but the soft magnetic pole tip, which is only 0.5 μm wide, tends to recess below the surrounding ceramic material. Since the head rides only 100 nm above the magnetic disk, it is desirable to keep the pole tip recession to less than 20 nm. An STM scan showing the recessed pole tip material (dark) and the lapping marks is shown in Fig. 3B. The STM is also used to evaluate the lapping process. The head was coated with titanium to make a conducting surface for STM. Electron microscopy cannot measure these small vertical distances, and optical interference techniques do not work because of the small width of the pole tip.

Other STM images with implications in the industrial world are shown in Fig. 3, C and D. The stampers that are used to manufacture compact disks (*23*) contain raised "bumps" that impress data into the disks (Fig. 3C). These bumps are about 130 nm high, 600 nm wide, and vary in length. In order to image the raised bumps, the feedback loop of the STM must be very fast so that the tip can follow the steep profiles without hitting the surface. These stampers are made of nickel and can be scanned without surface preparation. The sharpened edge of a diamond cutting tool (*24*) that is used for diamond turning of optical surfaces is shown in Fig. 3D. An ordinary diamond could not be imaged with the STM because it would not conduct electrons, but the diamond in Fig. 3D is a class 2B blue diamond that is slightly conducting and can thus be imaged with a platinum-iridium tip at a bias voltage of −2.4 V and a tunneling current of 0.4 nA.

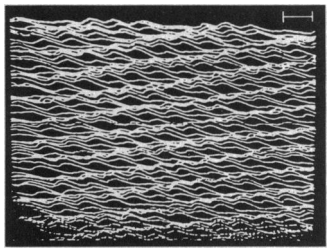

Fig. 4. Atomic-resolution image of a sample of graphite covered with water. Images such as this opened the possibility for electrochemists to image their electrodes without removing them from an electrochemical cell. The scale bar is 3 Å. [Figure from (*29*)]

These examples show how certain manufacturing processes can be understood and monitored by STM to provide quality control and guide the improvement of manufacturing procedures. The virtue of the STM in such applications is that as the dimensions of the objects become smaller, the STM scanning becomes even easier, whereas other techniques have already reached or exceeded their three-dimensional resolution limit. In the examples presented, the STM was used as an imaging tool, but the potential for other technological applications has raised considerable interest in which the STM would be used as a tool for manufacturing or repairing on a very small scale.

In a remarkable paper written more than 25 years ago, Feynman pointed out that if we can arrange atoms and molecules the way we want "we will get an enormously greater range of properties that substances can have, and of different things that we can do" (*25*). The STM has brought this dream much closer to reality. For example, Becker, Golovchenko, and Swartzentruber (*26*) have placed what appears to be a single atom onto a germanium surface. More recently, Foster, Frommer, and Arnett (*27*) have pinned an organic molecule in a particular location on a graphite surface. Even before atomic and molecular engineering applications become practical, the STM may be used for micrometer-scale jobs like the repair of (very expensive) masks for integrated circuit production (*28*).

Applications of the STM in Biology

When the resolution capabilities of the STM became evident, the possibility of examining biological structure in such detail was obvious and exciting. The discovery that STMs could be operated under water and other fluids (*29, 30*) opened the further possibility that biological substances could be examined in a near-native environment and with a probe that was nondestructive, conditions that are impossible for electron microscopy. Unfortunately, most materials of biological interest are not sufficiently conducting to allow STM images to be made. Although many are ionic conductors, almost none conduct electrons. For example, intracellular fluid can easily conduct electricity by the flow of ions, but it is a good insulator as far as electrons are concerned, which is why it has been possible to obtain atomic resolution images of conductors covered by water (*30*) and other fluids (*31*) (Fig. 4) (*29*).

The insulating properties of liquids have allowed electrochemists to obtain atomic resolution images of their electrodes in electrolytic solution (*32*), but these properties have limited the applications of STM in biology. For electrochemists, the STM images an electrode surface as if the electrolyte was not there. Electrons tunnel through

the electrolyte just as they would tunnel through a vacuum, so the images contain information about the electrode surface and not the electrolyte.

Our early attempts to image biological structures with STM met with dismal failure. For example, one of the first samples we tried to image was a plant leaf. Since the leaf was not a conductor for electrons, the tip advance mechanism simply pushed the tip right through the leaf until it came within tunneling distance of the conductive surface the leaf was mounted on. That underlying surface was imaged as if the leaf was not even there. Simply stated, a sample must conduct electrons if it is to be imaged by the STM, and most biological samples just do not conduct electrons at the required current levels—on the order of 10^{10} electrons per second in an area a fraction of a nanometer on a side.

One way to overcome the insulating nature of biomolecules is to apply an extremely thin conductive metallic coating and then image the metallic layer. For example, freeze-dried recA-DNA complexes coated with a 1-nm layer of a platinum-iridium-carbon alloy have been imaged by Amrein and co-workers (*33*). The coating had sufficient electron conductivity to be imaged with an STM and still allowed features as small as 2 nm to be revealed.

A related approach to overcoming the conductivity problem has been to make conductive metal replicas of insulating samples in much the same way as replicas are used for imaging biological materials with the transmission electron microscope (TEM) (*34*). A replica is made by depositing evaporated platinum and carbon (Pt-C) on the sample surface and then stripping the replica away from the sample or digesting the sample away with caustic liquids that do not affect the Pt-C layer. When such a replica is imaged with the STM, one takes care to image the surface of the replica that was in contact with the original sample in order to obtain the best resolution. In Fig. 5A an STM image reveals the inherent graininess of a Pt-C replica (*35*) of a freshly cleaved mica surface. The grains visible with STM mostly range from 0.8 to 3.5 nm in diameter and 0.2 to 1.2 nm in height. We have also imaged replicas of a protein, bovine catalase crystals, dried down onto a mica surface (Fig. 5B).

A further refinement of the replica technique is freeze-fracture replication, in which a hydrated sample is "fixed" by rapid freezing, then fractured to reveal surfaces at internal fracture planes. In Fig. 5, C and D, such replicas of the "ripple phase" of an artificial biomembrane composed of dimyristoylphosphatidylcholine (DMPC) are shown (*35*). Such replicas provide data on the height of the ripples. This combination of quantitative height profiles together with unsurpassed lateral resolution make the STM a valuable companion to the TEMs currently used for imaging replicas.

The advantage gained from the use of conductive metallic coatings and replicas does not come without some drawbacks, however. We must remember that with these techniques the STM creates images of the metal coatings and not of the original biological material. Thus the resolution is limited by the nature of the coating procedure and the topography of the grain in the metal surfaces. In fact, to our knowledge, there have not yet been any demonstrations of atomic detail in biological samples prepared by any method. Clearly, procedures for specimen preparation must receive considerable emphasis if the potential of the STM is to be realized for molecules of biological importance.

Many research groups have attempted to image biological samples directly, without making a replica. A limited number of biological macromolecules have been imaged with the STM, including DNA in vacuum and in water (*36*), bacteriophage ϕ29 (*37*), cell sheaths (*38*), and porin vesicles (*39*), but with limited resolution. Model membranes such as Langmuir-Blodgett films of cadmium arachidate have also been imaged (*40*). Other researchers abandoned their attempts to image biological materials directly after finding it difficult to obtain reproducible results. It is unclear what the mechanism of electron transport is through these materials. Perhaps there will be a class of materials that can be reproducibly and

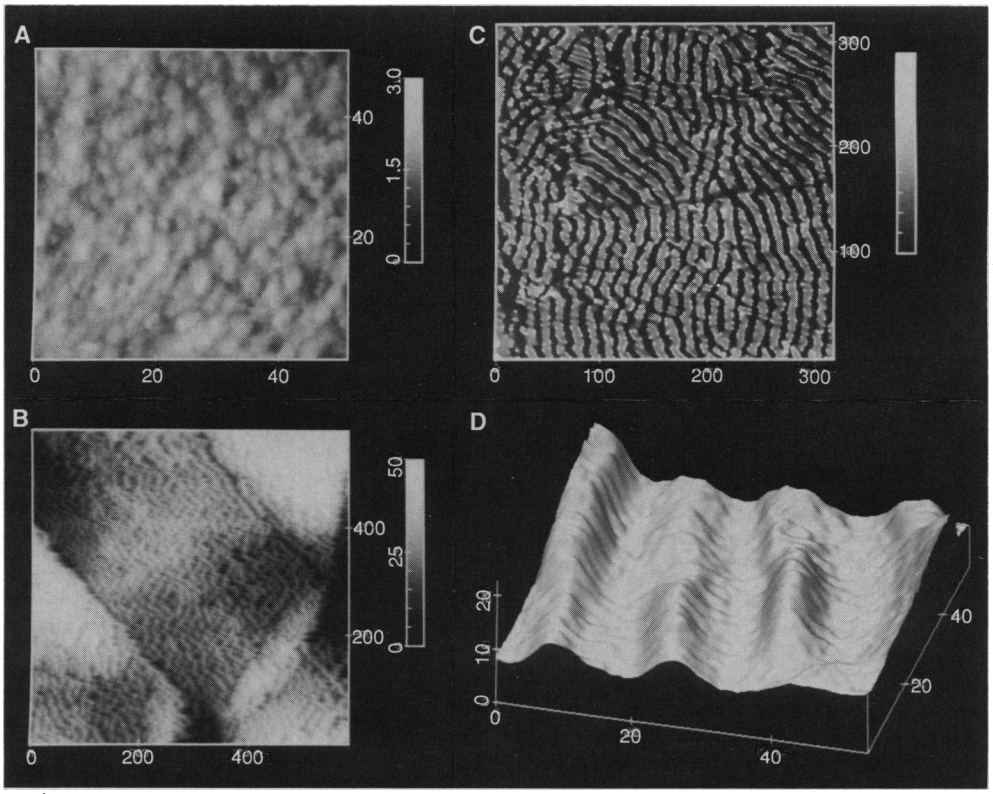

Fig. 5. Digital STM images of platinum-carbon (Pt-C) replicas (*35*). (**A**) Gray-scale representation of a replica of freshly cleaved mica (the surface shown is the Pt-C that was against the mica). Surface granulation ranges from 0.8 to 3.5 nm in diameter and 0.2 to 1.2 nm in height. Standard deviation in the z axis is 0.19 nm, and the maximum z range in this micrograph is 1.3 nm. Images such as this reflect the inherent graininess of the replica and not necessarily underlying structure of the surface to which it was applied. (**B**) Replica of a crystal of bovine catalase showing the surface of the crystal lattice. Catalase crystals in water suspension were dried down onto a mica surface, cooled to −105°C under vacuum, and coated with Pt-C. The catalase was then digested with sodium hypochlorite, and the side of the replica originally in contact with the catalase was imaged. (**C** and **D**) Filled surface views of a freeze-fracture replica of the $P_{\beta'}$ (ripple) phase of dimyristoylphosphatidylcholine [see (*35*)]. In the high-magnification view (D), the image has been inverted by computer so that the projection represents the topographic relations of the original freeze-fractured specimen, rather than the complementary surface of the replica. STM images such as these complement TEM images of similar specimens and reveal ripple amplitude as well as periodicity and form. The scales in all of these images are in nanometers.

fruitfully imaged with the STM. For example, it may be possible to learn about DNA conformation in water from studies such as those of Lindsay and colleagues (*36*). Unfortunately, however, it seems that the STM will not be a generally useful tool for imaging biological samples unless there are breakthroughs in sample preparation techniques or STM instrumentation.

Subtlety and Spectroscopy at High Magnification

If we are to interpret two spectacular images (discussed below) that point to an important part of the future of the STM, it is necessary to refine our understanding of STM images. The simple view that the images are topographs of surfaces has been sufficient so far. As shown in Fig. 6A, interpretations become more difficult for atomic resolution images of surfaces with inequivalent atoms. Note that the trajectory of the tip over the surface depends not only on the topography of the surface, but also on the types of atoms on the surface and the bias voltage used. Specifically, when the sample is negatively biased (switch in left position), the tip follows the dashed path and goes higher over the shaded atom than for positive sample bias voltage (switch in right position) when it follows the dot-dashed path. This response would occur for an atom with an excess of electrons. When the tip is over such an atom, the tunneling current flows readily from the atom with its excess of electrons to the tip, but not from the tip to the atom that does not readily accept more electrons. Thus current flows readily when the sample is negative; then the feedback network moves the tip away from the surface to reduce the current to the preset value. Conversely, the current does not flow readily when the sample is positive; then the feedback network moves the tip toward the sample to increase the current to the preset value.

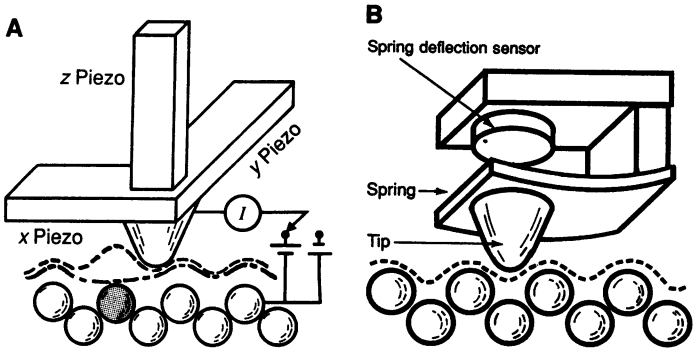

Fig. 6. Schematic diagrams comparing important differences between the operation of an STM and an AFM. (**A**) An STM actually traces contours of constant electron density at a particular energy determined by the bias voltage. Thus, when there are different atoms in a surface layer, atomic resolution images will depend on bias voltage. For example, the shaded atom would differ from the other atoms by more readily giving up electrons for tunneling (sample bias negative) and less readily accepting them (sample bias positive). Two different paths that the tip would follow over the surface for two different bias voltages indicated by the two batteries and switch are shown (sample bias negative for the dashed line; sample bias positive for the dot-dashed line). (**B**) Schematic view of the force sensor for an AFM. The essential features are a tip, shown as a rounded cone, a spring, and some device to measure the deflection of the spring. In practice, the spring deflection sensor can be either based on electron tunneling to the back of the spring, on optical interference between the back of the spring and a reference plate, or by deflection of a laser-light beam reflected off the back of the spring. In any case, the tip follows a path (dashed line) that is an accurate topograph of the surface. The voltage dependence effect, displayed in (A) for the STM, is not present here. Indeed, no voltage is applied between the tip and the sample, and no current needs to flow between the tip and the sample. Thus the AFM can image nonconducting samples.

In an actual STM image, the shaded atom would appear as a large bump on the sample for a negative sample bias voltage and as a dip for positive sample bias voltage. As an example, in Fig. 7 adsorbed oxygen on a gallium arsenide surface appears as a large bump for negative sample bias voltage and as a hole for positive sample bias voltage (*41, 42*).

A more precise explanation is that the tip of an STM follows contours of constant electron density at a particular energy (*43, 44*). That energy is determined by the bias voltage of the tip. Calculations based on this principle have been published for a number of surfaces, including gold (*43*), graphite (*45*), and silicon (*46*). Comparison of detailed calculations and high-resolution experimental images of TTF-TCNQ (tetrathiafulvalene-tetracyanoquinodimethane) (Fig. 8) (*47*) reveals the subtlety of detail possible with calculations that take into account the molecular orbitals that are available for conduction at a particular tip bias voltage.

In some cases the tip can be stopped over a single atom, and the tip bias voltage can be varied to do spectroscopy (*48*). For example, Wolkow and Avouris recently published electron spectra obtained in this way for a tip over various sites on a silicon surface that had been exposed to NH_3 (*49*). Subtle details about electron transfer between various inequivalent sites on the surface were inferred. Clearly, there is an opportunity for obtaining tremendously detailed, site-specific information on electronic states for technologically important systems.

The Atomic Force Microscope

The AFM, a very recent invention (*5*), produces images that are much closer to simple topographs and can image nonconducting surfaces (*5–9*). Thus, it has promise for imaging biological materials and other substances that do not readily conduct electrons.

The AFM records interatomic forces between the apex of a tip and atoms in a sample as the tip is scanned over the surface of the sample (Fig. 6B). When the AFM is operated in a mode that senses the repulsive forces between tip and sample, the tip actually touches the sample, much like the stylus of a record player touches the surface of a record. For the AFM, however, the tip is much sharper and the tracking force is much smaller: about one-millionth as great as for a record player. At these small tracking forces, the tip can trace over individual atoms without damaging the surface of the sample. The AFM can also be operated so that it senses the attractive forces between the tip and the sample. The feedback system then prevents the tip from touching and damaging the sample. But this mode of operating an AFM comes at the cost of decreased lateral resolution. So far, most images obtained in this way are of micrometer-scale objects.

The tip can be made of a small fractured diamond fragment attached to a spring in the form of a cantilever (*50*). The small repulsive tracking forces between the tip and the sample, usually in the range of 10^{-6} to 10^{-9} N, are recorded by measuring minute deflections of the cantilever. A typical spring constant for a cantilever would be about 1 N/m, which is roughly the spring constant of the popular children's toy called a "Slinky," or of a piece of household aluminum foil 3 mm long and 1 mm wide. If a deflection as small as 1 nm can be sensed for a cantilever with a spring constant of 1 N/m, then a tracking force as low as 10^{-9} N can be applied between the tip and the sample. Clearly, this would be impossible for a "Slinky" because its large mass makes its vibrational frequency so low that it is strongly affected by vibrations in the room. However, a very small cantilever made of aluminum foil or other suitable material is much less sensitive to vibrations because its resonant frequency is about 1 kHz in contrast to 1 Hz for the

"Slinky." Microcantilevers made of silicon oxide with silicon etching technology (*51*) are even lighter and have resonant frequencies as high as 100 kHz. The higher the resonant frequency, the less sensitive the cantilever is to vibrations, and the more stable it is for atomic force microscopy. The vibration of one end of the cantilever relative to the other in response to an external vibration of magnitude A and frequency ν is approximately $A(\nu/\nu_r)^2$, where ν_r is the resonant vibration frequency of the cantilever (*52*). For a typical laboratory room, A would be of order 1 μm and ν_r of order 20 Hz. Thus a cantilever with a vibrational frequency of 10 kHz would have a vibration amplitude less than 0.01 nm and be suitable for atomic resolution imaging with minimal vibration isolation.

An AFM can be designed to look very similar to an STM (Fig. 2B). The primary difference is that it is convenient to have the sample move rather than the delicate, and sometimes bulky, force sensor (composed of tip, spring, and spring deflection sensor; Fig. 6B). Such an AFM can be used as an STM by simply replacing the force sensor with a tunneling tip (*53*).

The deflection of the spring in the force sensor can be measured with electron tunneling (*5*), an interferometer (*54*), or by the deflection of a laser beam reflected off a mirror mounted on the back of the spring (*55*). All that is required is an electrical signal that varies rapidly with the deflection. This signal is sent to the same type of electronics used for STM. Specifically, a feedback circuit controls the voltage applied to a z piezo element so that the signal is held constant as the tip is scanned across the surface of the sample with the x piezo. As for the STM, one scan is a plot of the voltage applied to the z piezo as a function of the voltage applied to the x piezo. Images are composed of multiple scans, each displaced in the y direction from the previous one.

Applications of the AFM

Many atomic-resolution images have already been produced by AFMs. The first published atomic-resolution image of a nonconductor was of boron nitride (Fig. 9) (*56*). The AFM has also been used successfully to image surface detail of organic nonconducting mate-

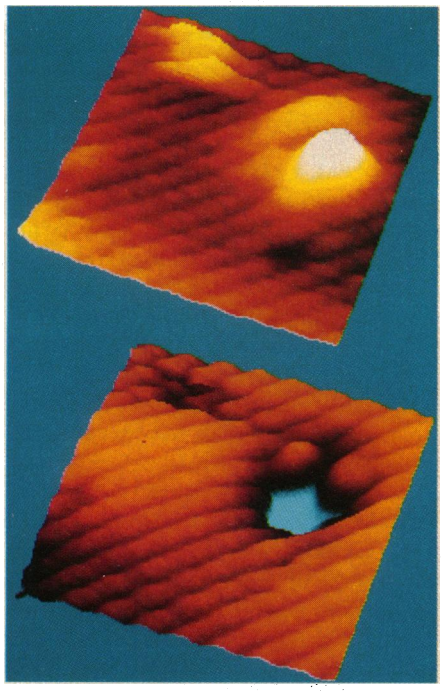

Fig. 7. STM images of an oxygen defect on n-GaAs (110) acquired simultaneously at sample voltages of (**top**) −2.6 V and (**bottom**) 1.5 V. [Data from Stroscio, Feenstra, and Fein (*41*). Image coloring by R. Freemine, National Bureau of Standards, Gaithersburg, Maryland]

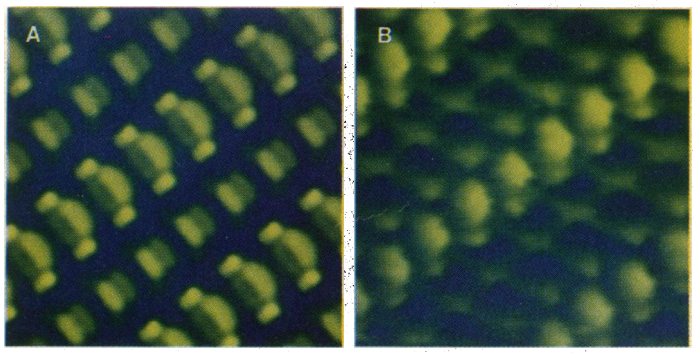

Fig. 8. This comparison of (**A**) theory and (**B**) experiment for STM images of the organic conductor TTF-TCNQ illustrates the subtlety of molecular orbitals that can be imaged with an STM. [Figure from (*47*), courtesy of *Physical Review Letters*]

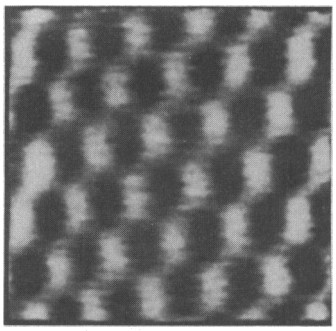

Fig. 9. This AFM grey-scale image of boron nitride was the first atomic resolution image of a nonconductor. The field shown is 1.2 nm wide. [Figure from (*56*), courtesy of *The Journal of Applied Physics*]

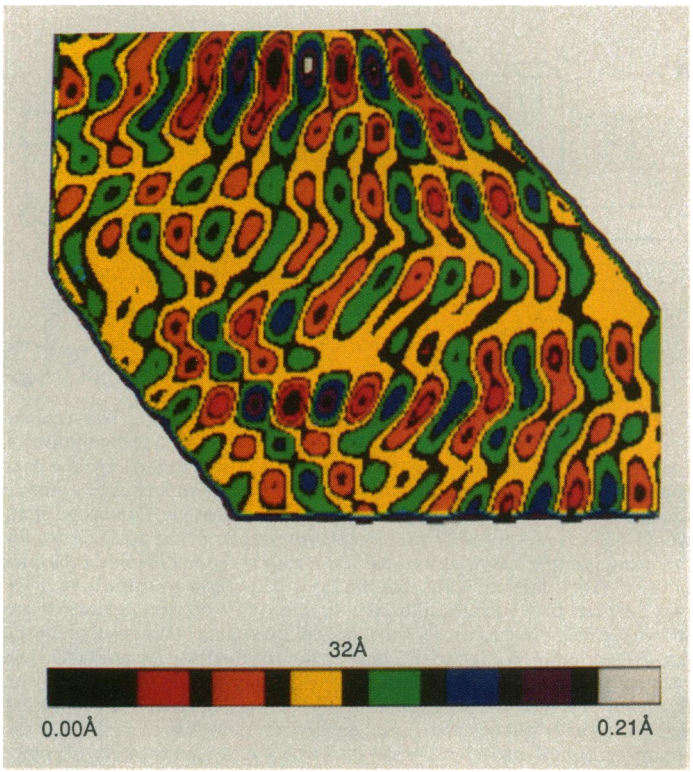

Fig. 10. AFM image of a polymerized monolayer *n*-(2-aminoethyl)-10,12-tricosadiynamide reveals parallel rows of molecules with a side-by-side spacing of ~0.5 nm. Forces used for imaging (10^{-8} N) had no observable effect on the polymer strands. These results demonstrate that AFM images can be obtained for an organic system. [Figure from (*57*)]

rials. In Fig. 10 the parallel rows with 0.5-nm spacing represent a polymerized molecular monolayer of *n*-(2-aminoethyl)-10,12-tricosadiynamide (*57*). This image was obtained with a tracking force of about 10^{-8} N, which was barely small enough to prevent the monolayer from being disrupted. Although the monolayer could be imaged repeatedly, it was finally damaged after tens of images were obtained.

We have also imaged the surface of crystals of the amino acid DL-leucine (see cover) with an AFM (*58*). The white dots in the computer-processed image represent topographic peaks of methyl groups at the end of individual DL-leucine molecules. The positions of the methyl groups in this molecular crystal agree with the positions predicted from x-ray diffraction analysis of the sample, demonstrating that the surface is a simple termination of the bulk.

It is encouraging that we have been able to image the polymerized monolayer and the amino acid crystal, because they are much softer than boron nitride, graphite, MoS_2, and other inorganic materials that have been imaged with the AFM. However, they are still more rigid than biological structures such as proteins. Physical rigidity is one of the important properties a material must have for successful imaging by AFM. Smaller tracking forces, perhaps in the 10^{-10} N range or less, may be necessary to image these fragile structures. One possibility now under study is to use the AFM at very low temperatures to take advantage of the rigidity inherent in frozen biological structures.

For proper perspective, it is important to remember that the AFM is a new instrument and that its development is still in the early stages. Technology for the STM began earlier and has progressed to the point that STMs are now used as routine tools in many laboratories and for many purposes. In contrast, there are no commercially available AFMs, and the few that exist in research laboratories work only occasionally at high resolution. The main difficulties with AFMs seem to be in: (i) reproducibly measuring the minute deflections of the cantilevers, (ii) producing cantilevers with high resonant frequencies that are robust and large enough to locate with a tunneling tip or other device for measuring deflection, and (iii) reproducibly producing sharp tips and keeping them clean. When these obstacles have been substantially overcome, it should be possible to turn more attention to methods of specimen preparation so that the range of information accessible to AFMs can be explored. But in spite of these problems, we note with optimism that the evolution of the AFM has been much more rapid than the evolution of the STM, in part because of the experience that has been gained in building and using STMs, and in part because of the importance of developing microscopes that can image nonconducting surfaces directly.

Although AFMs are new, we have not given a complete overview here, but have picked only a few examples. Other important examples include atomic-scale friction measurements (*59*), imaging of magnetic fields above thin-film recording heads (*60*), and imaging of a photoresist on silicon (*61*).

Outlook

What is the outlook for STM and AFM in technology and biology? For technology, both instruments should become useful tools for monitoring and evaluating critical manufacturing processes. In time, the hope that manipulative processes will be possible in the nanometer range with STMs or related scanning probes may also be realized. It is certainly worth further exploration.

For biology, the picture is much less clear. The recent upsurge of interest and applications of the STM in physics and engineering research is the result of dramatic breakthroughs in instrumentation and invention in the last few years. But the interest in biological applications has not been accompanied by comparable advances in methods for preparing and examining specimens. The biologist who seeks to exploit the potential of the STM faces many challenging obstacles before this instrument can be applied as a routine tool to generate information that is unavailable to other, more traditional microscopes. This is not to dampen the spirits of those who wish to try, but just to be realistic; there is a large gulf between the possibility and the payoff of successful practical application. Our interest in biological applications remains high, whether the best successes will eventually come from STM, AFM, or other scanning probes in the future.

We think several obstacles deserve special mention in the hope that innovative solutions can be found to overcome them. First among these, at least for the STM, is the poor electron conductivity of most biological molecules, for without the ability to conduct electrons, there can be no image from electron tunneling. Occasional exceptional specimens may arise from time to time and offer hope, but they will be of limited use unless they represent broadly applicable mechanisms.

The application of metals to make conductive coatings or replicas presently has limited usefulness. The obvious advantage over more conventional microscopes is that the STM can easily determine height, or z information, in these samples. But the drawback is that a replica is not original structure, and it is not realistic to hope for resolution at the level of atoms or small molecules with such methods. To date we know of no STM micrographs of biological molecules prepared by any method that approach the atomic-scale resolution that is possible with more ideal materials. That is why alternative instruments such as the AFM, which has already demonstrated atomic and molecular resolution images of nonconducting samples, are potentially so important.

Many important opportunities remain for further advances in instrument design and specimen preparation. Among these are: (i) extending the scanning range of microscopes and incorporating x-y translation stages to help locate and identify features of interest; (ii) further development of scanning probe microscopes designed to image soft nonconductors; (iii) finding ways to anchor biological samples, make them mechanically stable, and control their orientation and distribution; (iv) learning to recognize target features among populations by use of reliable markers; and (v) avoiding artifacts caused by preparative methods.

Scanning probe microscopy is a young field that is still in the early stages of development and application. The advantages of obtaining high-resolution information with virtually nondestructive probes has been, and will continue to be, appealing for biologists and others. We have covered only a few examples of recent applications; one important area we did not include is the study of dynamic processes, such as corrosion (*62*). Perhaps the greatest potential for scanning probe microscopes in biology will go beyond the recording of static images as new probes are developed that may be capable of sensing different kinds of signals to reveal the dynamics of biological processes at the submicron level.

Note added in proof: New AFMs that use fiber optic interferometers to sense the deflection of the spring in the force sensor have been developed by scientists at IBM Almaden Research Center. Important technological applications have already been made there: for example, imaging magnetization patterns on magnetic disks and measuring lubricant thicknesses on surfaces.

We now believe that these new AFMs, and others that use light to sense the deflection of the spring (*54, 55, 59–61*), are preferable to AFMs that use electron tunneling to sense the deflection. They are more reliable and yield more reproducible results because they are much less sensitive to contamination on the spring.

REFERENCES AND NOTES

1. G. Binnig, H. Rohrer, Ch. Gerber, E. Weibel, *Phys. Rev. Lett.* **49**, 57 (1982).
2. For two excellent short reviews of STM, see C. F. Quate, *Physics Today* **39**, 26 (August 1986), and J. A. Golovchenko, *Science* **232**, 48 (1986).
3. For a longer review, see P. K. Hansma and J. Tersoff, *J. Appl. Phys.* **61**, R1 (1987).
4. The STM'87 Conference Proceedings (about 75 papers) were edited by R. Feenstra and published in *J. Vac. Sci. Technol. A* **6**, 259–556 (1988).
5. G. Binnig, C. F. Quate, Ch. Gerber, *Phys. Rev. Lett.* **56**, 930 (1986).
6. AFMs are so new that there are not, to our knowledge, any reviews in print. The eight papers in the AFM session of the STM'87 Conference Proceedings provide an overview; see pp. 266–295 in (*4*).
7. A recent review is Y. Martin, C. C. Williams, H. K. Wickramasinghe, *Scanning Microscopy* **2**, 3 (1988).
8. The first atomic-resolution STM image is in G. Binnig, H. Rohrer, Ch. Gerber, E. Weibel, *Phys. Rev. Lett.* **50**, 120 (1983).
9. The first atomic resolution AFM image is in G. Binnig *et al.*, *Europhys. Lett.* **1**, 31 (1986).
10. For a discussion of theoretical work on single-atom imaging, see N. D. Lang, *Phys. Rev. Lett.* **55**, 230 (1985); *ibid.* **56**, 1164 (1986).
11. The Nobel Prize acceptance speech is in G. Binnig and H. Rohrer, *Rev. Mod. Phys.* **59**, 615 (1987).
12. For examples, see R. M. Tromp, R. J. Hamers, J. E. Demuth, *Phys. Rev. B* **34**, 1388 (1986); and J. A. Golovchenko in (*2*).
13. See, for example, R. M. Feenstra and A. P. Fein, *Phys. Rev. B* **32**, 1394 (1985), and references therein.
14. See, for example, the six papers on graphite in the section on STM of layered materials, pp. 336–375, of the STM'87 conference proceedings (*4*).
15. Nanoscope, Digital Instruments, Inc., Santa Barbara, CA.
16. W.A. STM, WA Tech. Ltd., Cambridge, England; STM, McAllister Technical Services, Berkeley, CA; STM, Microscience, Inc., Braintree, MA; STM, VG Instruments, Stanford, CA.
17. Usually the piezoelectric material is a lead titanate–lead zirconate ceramic.
18. B. Drake, R. Sonnenfeld, J. Schneir, P. K. Hansma, *Surf. Sci.* **181**, 92 (1987). A refined version of this design is available commercially (*15*).
19. D. P. E. Smith and G. Binnig, *Rev. Sci. Instrum.* **57**, 1688 (1986).
20. W. J. Kaiser and R. C. Jaklevic, *Surf. Sci.* **181**, 55 (1987).
21. Perkin-Elmer Corp., Irvine, CA. All of the images in Fig. 3 were obtained with a commercial STM, the Nanoscope II (*15*).
22. Censtor Corp., San Jose, CA.
23. Sanyo Corp., Tokyo, Japan.
24. R. Day, Los Alamos Scientific Laboratory, Los Alamos, NM.
25. R. P. Feynman, in *Miniaturization*, H. D. Gilbert, Ed. (Reinhold, New York, 1961), pp. 282–296.
26. R. S. Becker, J. A. Golovchenko, B. S. Swartzentruber, *Phys. Rev. Lett.* **55**, 987 (1985).
27. J. Foster, J. E. Frommer, P. C. Arnett, *Nature* **331**, 324 (1988). See also J. B. Pethica, *ibid.*, p. 301.
28. R. Wickramasinghe, personal communication.
29. R. Sonnenfeld and P. K. Hansma, *Science* **232**, 211 (1986).
30. H. Y. Liu, F.-R. F. Fan, C. W. Lin, A. J. Bard, *J. Am. Chem. Soc.* **108**, 3838 (1986).
31. J. Schneir and P. K. Hansma, *Langmuir* **3**, 1025 (1987).
32. For an example of imaging electrodeposition and stripping, see R. Sonnenfeld and B. Schardt, *Appl. Phys. Lett.* **49**, 1172 (1986); Two examples of imaging on an electrode while it is held under potential control are O. Lev, F. R. Fan, A. J. Bard, *J. Electrochem. Soc.* **135**, 783 (1988), and P. Lustenberger, H. Rohrer, R. Christoph, H. Siegenthaler, *J. Electroanal. Chem.* **243**, 225 (1988).
33. M. Amrein, A. Stasiak, H. Gross, E. Stoll, G. Travaglini, *Science* **240**, 514 (1988).
34. In typical TEM studies, metal is evaporated and directed at the sample from an elevation of 45° or less so that differences in thickness of metal pile-up on the specimen are seen as contrast differences in the TEM. For STM, the metal is evaporated from above, normal to the main sample plane, so that the specimen is uniformly coated with a continuous conducting layer and there are no "shadow pockets" lacking metal.
35. All the replicas shown in Fig. 5 were made in J. Zasadzinski's laboratory at UCSB with a Reichert-Jung Cryofract 190 freeze-fracture apparatus (Cambridge Instruments, Buffalo, NY) and imaged with a commercial STM, the Nanoscope II (*15*). Figure 5D is from J. A. N. Zasadzinski *et al.*, *Science* **239**, 1013 (1988).
36. See figure 36 in (*3*); S. M. Lindsay and B. Barris, *J. Vac. Sci. Technol. A* **6**, 544 (1988); B. Barris, U. Knipping, S. M. Lindsay, L. Nagahara, X. X. Thundat, *Biopolymers* **27**, 1691 (1988).
37. A. M. Baró *et al.*, *Nature* **315**, 253 (1985).
38. D. C. Dahn, M. O. Watanabe, B. L. Blackford, M. H. Jericho, *J. Vac. Sci. Technol. A* **6**, 548 (1988).
39. A. Stemmer *et al.*, *Surf. Sci.* **181**, 394 (1987).
40. D. P. E. Smith *et al.*, *Proc. Natl. Acad. Sci. U.S.A.* **84**, 969 (1987); C. A. Lang, J. K. H. Hörber, T. W. Hänsch, W. M. Heckl, H. Möhwald, *J. Vac. Sci. Technol. A* **6**, 368 (1988).
41. J. A. Stroscio, R. M. Feenstra, A. P. Fein, *Phys. Rev. Lett.* **58**, 1668 (1987).
42. J. A. Stroscio, R. M. Feenstra, D. M. Newns, A. P. Fein, *J. Vac. Sci. Technol. A* **6**, 499 (1988).
43. J. Tersoff and D. R. Hamann, *Phys. Rev. Lett.* **50**, 25 (1983).
44. ———, *Phys. Rev. B* **31**, 2 (1985).
45. A. Selloni, P. Carneveli, E. Tosatti, C. D. Chen, *ibid.* **31**, 2602 (1985); J. Tersoff, *Phys. Rev. Lett.* **57**, 440 (1986).
46. See R. M. Tromp *et al.* in (*12*).
47. T. Sleator and R. Tycko, *Phys. Rev. Lett.* **60**, 1418 (1988).
48. See, for example, R. M. Tromp, R. J. Hamers, J. E. Demuth, *Science* **234**, 304 (1986), and references therein.
49. R. Wolkow and Ph. Avouris, *Phys. Rev. Lett.* **60**, 1049 (1988).
50. The diamond can be a fragment from a small gem (we got our first from a pawnshop for $7) that is shattered with a hammer between two pieces of hardened steel.
51. T. R. Albrecht and C. F. Quate, *J. Vac. Sci. Technol. A* **6**, 271 (1988).
52. This formula, which can be easily derived as the low-frequency limit of the vibration transmission formula found in mechanical engineering texts, is multiplied by a constant of order unity that depends on the damping. For example, for velocity dependent damping the constant is $1-2\delta^2$, where δ is the ratio of the damping to the critical damping.
53. For photographs of an AFM-STM, see O. Marti, B. Drake, S. Gould, P. K. Hansma, *J. Vac. Sci. Technol. A* **6**, 287 (1988).
54. R. Erlandsson, G. M. McClelland, C. M. Mate, S. Chiang, *J. Vac. Sci. Technol. A* **6**, 266 (1988), and references therein.
55. N. M. Amer and G. Meyer, *Bull. Am. Phys. Soc.* **33** (no. 3), 319 (1988); G. Meyer and N. M. Amer, *Appl. Phys. Lett.* **53**, 1045 (1988).
56. T. R. Albrecht and C. F. Quate, *J. Appl. Phys.* **62**, 2599 (1987).
57. O. Marti *et al.*, *Science* **239**, 50 (1988).
58. S. Gould *et al.*, *Nature* **332**, 332 (1988).
59. C. M. Mate, G. M. McClelland, R. Erlandsson, S. Chiang, *Phys. Rev. Lett.* **59**, 1942 (1988).
60. Y. Martin and H. K. Wickramasinghe, *Appl. Phys. Lett.* **50**, 1455 (1987).
61. Y. Martin, C. C. Williams, H. K. Wickramasinghe, *J. Appl. Phys.* **61**, 4723 (1987).
62. B. Giambattista *et al.*, *Proc. Natl. Acad. Sci. U.S.A.* **84**, 4671 (1987).

63. We thank R. V. Coleman and his students, J. Demuth and his group, B. Drake, M. Eddy, S. Gould, J. Gurley, L. Hellemans, N. Keder, C. Quate and his students, J. Schneir, K. Shaw, R. Sonnenfeld, G. Stuckey, C. M. Wu, and J. Zasadzinski for their contributions to the research discussed in this article, S. Gould and J. Zasadzinski for reading and improving this article, and, of course, the authors from other institutions who contributed the referenced figures. Supported in part by the National Science Foundation, Solid State Physics grant DMR86-13486 (P.H.) and by the Office of Naval Research (O.M.). It is journal paper number 11,721 of the Purdue University Agricultural Experiment Station.